A window into the Proterozoic: Integrating 3D seismic, gravity, and magnetic data to image subbasement structures in the southeast Fort Worth basin

Murari Khatiwada[1], G. Randy Keller[1], and Kurt J. Marfurt[1]

Abstract

The Fort Worth basin (FWB) is one of the most fully developed shale gas fields in North America. Although there are hundreds of drilled wells in the basin, almost none of them reach the Precambrian basement. Imaged by perhaps 100 3D seismic surveys, the focus on the relatively shallow, flat-lying Barnett Shale objective has resulted in little published work on the basement structures underlying the Lower Paleozoic strata. Subtle folds and systems of large joints are present in almost all 3D seismic surveys in the FWB. At the Cambro-Ordovician Ellenburger level, these joints are often diagenetically altered and exhibit collapse features at their intersections. We discovered how the basement structures relate to overlying Paleozoic reservoirs in the Barnett Shale and Ellenburger Group. In support of our investigation, the Marathon Oil Company provided a high-quality, wide-azimuth, 3D seismic data near the southeast fringe of the FWB. In addition to the seismic volume, we integrated the seismic results with gravity, magnetic, well log, and geospatial data to understand the basement and subbasement structures in the southeast FWB. Major tectonic features including the Ouachita frontal thrust belt, Lampasas arch, Llano uplift, and Bend arch surround the southeast FWB. Euler deconvolution and integrated forward gravity modeling helped us extend our interpretation beyond the 3D seismic survey into a regional context.

Introduction

The Fort Worth basin (FWB) is a Late Paleozoic foreland basin that is associated with the Ouachita orogenic belt (OOB) and occupies an estimated area of about ~ 38,000 km^2 (15,000 sq. mi) (Montgomery et al., 2005; Pollastro et al., 2007; Bruner and Smosna, 2011). Major tectonic units that bound the FWB include the Muenster arch that is related to the Southern Oklahoma aulacogen (SOA), the Llano uplift (LU), the Ouachita frontal thrust belt (OFTB), and the Bend arch (Figure 1). The FWB was primarily developed during the Early and Middle Pennsylvanian in front of the advancing Ouachita fold belt (Walper, 1982; Kruger and Keller, 1986; Pollastro et al., 2007).

Tectonic studies of the FWB and its surrounding regions, such as the OOB, and the LU, date back as early as 1857 (Viele, 1989). Flawn (1961) publishes a notable summary about the geologic and tectonic history of the entire OOB. After the emergence of plate tectonics, studies of the region escalated and numerous regional analyses of the tectonic and geologic evolution of the Ouachita system were undertaken (e.g., Nicholas and Rozendal, 1975; Kruger and Keller, 1986; Arbenz, 1989, 2008; Denison, 1989; Keller et al., 1989; Nicholas and Waddell, 1989; Viele 1989; Viele and Thomas, 1989). The LU is important because it is the only Precambrian basement outcrop in the region; studies of its structure and evolution include Carter (1989), Mosher et al. (2008), Barker and Reed (2010), and Levine and Mosher (2010). Regional geophysical studies of the FWB region include Nicholas and Rozendal (1975) who use 2D seismic, gravity, and geologic data to interpret the subsurface structures within the Ouachita fold belt and their relation to the Paleozoic cratonic margin. Kruger and Keller (1986) use gravity, drilling, and geologic data to study the crustal structure of Ouachita Mountains and FWB region. The crustal scale structure of the region was synthesized by Mickus and Keller (1992) who use 2D seismic refraction and reflection profiles from COCORP and PASSCAL scientific experiments, well data, and gravity data to interpret the lithospheric structure of the OFTB across the Gulf coastal plain, to the Gulf of Mexico.

The geologic framework, history, and tectonic evolution of the FWB are discussed in many publications such as Henry (1982), Walper (1982), Meckel et al.

[1]ConocoPhillips School of Geology and Geophysics, University of Oklahoma, Norman, Oklahoma, USA. E-mail: khatiwada1@gmail.com; grkeller@ou.edu; kmarfurt@ou.edu.

Manuscript received by the Editor 22 March 2013; published online 7 October 2013. This paper appears in *Interpretation*, Vol. 1, No. 2 (November 2013); p. T125–T141, 15 FIGS.

http://dx.doi.org/10.1190/INT-2013-0041.1.

(1992), Thomas and Texas (2003), Erlich and Coleman (2005), Montgomery et al. (2005), Loucks and Ruppel (2007), Pollastro et al. (2007), and Bruner and Smosna (2011). Hardage et al. (1996) use 3D seismic data to study the relationships between the karst and collapse features and overlying clastic stratigraphy. Since these studies, potential field data; drilling results; and volumetric seismic attributes such as dip and azimuth, curvature, coherence, and reflector parallelism of convergence have been widely used to identify and interpret small to megascale structural features in the subsurface and their relation to the bounding rock units. For example, Sullivan et al. (2006) successfully use volumetric seismic attributes such as curvature, coherence, and reflector rotation to map chimneys, collapse, and karst features of the Ellenburger Group in the FWB and showed that these features are controlled by tectonic processes. Aktepe et al. (2008) use volumetric attributes such as coherence and curvature to map and analyze basement faulting and show their involvement with the observed collapse features in the Paleozoic strata above the basement. Elebiju et al. (2010) use volumetric seismic attributes and high-resolution aeromagnetic data to successfully establish links between the Precambrian basement structure and sedimentary structures of overlying Paleozoic strata in the northern part of the FWB.

Most of the recent geophysical studies in the FWB are focused on the northern part because of the presence of thicker Barnett Shale and other oil and gas bearing carbonate units. Geophysical studies and published

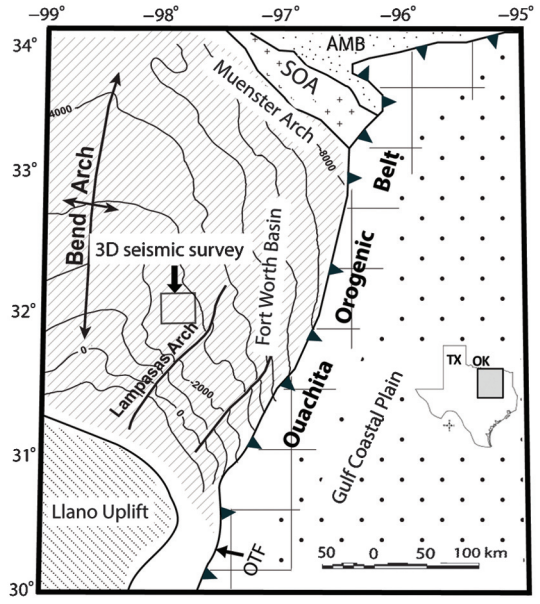

Figure 1. Index map of the study area showing FWB and major tectonic units surrounding it, modified after Ewing et al. (1990), Pollastro et al. (2007), and Keller (2009). The boundaries of the OOB, LU, SOA, Ardmore-Marietta basin, and Ouachita thrust front (OTF) are based on observed gravity anomalies. Contours represent the depth to the top of Ellenburger Group with an interval of ~305 m (1000 ft).

works in the southern FWB are limited because of the reduced thickness of the Barnett Shale and absence of the key Paleozoic carbonate units such as the Viola, Simpson, and Forrestberg Limestone (Montgomery et al., 2005; Pollastro et al., 2007; Bruner and Smosna, 2011). Although there are hundreds of oil and gas exploration and production wells, most are focused on the shallow Barnett Shale production such that we lack well data below the Cambro-Ordovician Ellenburger Group. There is even less data and fewer published studies on the basement structures of the southern FWB.

This study is focused on the data sparse southern FWB, where Marathon Oil Company collected 3D seismic data in a small area of Hamilton County, Texas in 2006 (Figure 1). We used these 3D seismic data to identify and interpret basement and subbasement structures and their relationship with the overlying Paleozoic and Late Paleozoic sequences. We augmented this proprietary data volume with publicly available gravity, magnetic, and geospatial data. We integrated the results obtained from these geophysical methods to understand the details of the Precambrian basement in the southeast FWB. We also constructed an integrated forward gravity model across the FWB and OFTB and performed Euler deconvolution of the magnetic data. Afterward, we integrated the results to interpret the tectonic and structural history of the basement and its relationship with the overlying basin.

Geologic and tectonic background

The Phanerozoic evolution of the area started with Early Paleozoic continental rifting in the context of a Wilson Cycle that formed the SOA and the Early and Middle Paleozoic continental margin along which the OOB developed in the Late Paleozoic (e.g., Keller, 2009). The FWB was part of the southern Laurentian passive margin when Laurentia collided with Gondwana in the Middle Paleozoic (Dalziel et al., 1994; Dennie, 2010). The Paleozoic Ellenburger Group, Simpson Group, and Viola Limestone lie beneath a major unconformity and are overlain by the Forrestberg Limestone, Barnett Shale, and Marble Falls Limestone Group. Pennsylvanian strata subsequently filled the FWB. Today, Proterozoic rocks are exposed in the LU area. The west and northwest portions of the FWB are covered with Paleozoic rocks, whereas the OOB, eastern FWB, and the Gulf Coastal Plain (GCP) are all covered with Cretaceous and Quaternary sediments (Figure 1). Walper (1982) interprets some high angle normal faults and graben structures in the FWB mostly associated with the Ouachita orogenic fold-thrust belt and the LU. Some of these faults are exposed, but most of them are buried under the Quaternary sediments.

The FWB is bounded on the east by the OOB, which is the most prominent structure in the periphery of the basin and forms the approximate boundary between the transitional crust of the Gulf of Mexico and the cratonal North America (e.g., Kruger and Keller, 1986; Keller et al., 1989; Gao et al., 2008). The Ouachita Mountains

have limited exposure in Texas and are buried beneath the younger Cretaceous and Quaternary sediments (Keller and Cebull, 1973; Keller et al., 1989; Viele, 1989; Viele and Thomas, 1989). The Ouachita orogeny started in the Late Paleozoic when a southern continent collided with North America; the tectonic activity migrated westward and ended by the Early Permian (Kruger and Keller, 1986; Keller and Hatcher, 1999). The inboard side (the side toward the FWB) of the OFTB contains unmetamorphosed to slightly metamorphosed preorogenic offshore and synorogenic deep-water rocks, whereas the outboard side contains higher grade metamorphic rocks (Flawn, 1961; Viele, 1989). The north border of the basin, the Muenster arch, is a fault-bounded basin uplift related to the SOA, which was reactivated during the Ouachita orogenic compression (Walper, 1982; Keller et al., 1989; Pollastro et al., 2007; Elebiju et al., 2010). The FWB is bounded by the Bend arch in the west, which is a subsurface structural high that extends north of the LU. In the Late Mississippian, the FWB subsided and tilted westward, which is one of the reasons for the formation of the Bend arch (Tai, 1979; Walper, 1982; Pollastro et al., 2007). The FWB is terminated on the south by the LU, which is a dome-shaped structural feature that exposes Mesoproterozoic-Paleozoic rocks (Montgomery et al., 2005; Pollastro et al., 2007; Mosher et al., 2008). The rocks in the northeast portion of the LU are deformed and metamorphosed with many northeast–southwest-trending normal faults related to the Ouachita orogenic event (Smith, 2004; Mosher et al., 2008). The Lampasas arch is another prominent structure in the southern FWB that extends northeast from the LU and follows the orientation of other major faults related to the Ouachita frontal zone (Pollastro et al., 2007). In addition to these major structures, many basement-related normal faults, thrust faults, fractures, karst, and collapse features are abundantly found in the Cambrian to Pennsylvanian units throughout the FWB. These structures relate to multiphase tectonic events. Some of these structures were reactivated in the north and northeast part of the basin, however, the direction and orientation of these structures changes rapidly from place to place (Flawn, 1961; Henry, 1982; Pollastro et al., 2003; Montgomery et al., 2005; Pollastro et al., 2007). Due to these different tectonic events, the FWB formed as an asymmetrical and wedge-shaped basin that pinches out toward the south (Figure 1).

General stratigraphy

The generalized stratigraphy of the FWB is shown in Figure 2. The basement of the FWB is made up of structurally complex Precambrian metasediments, granite, diorite, gneiss, and schist (Preston et al., 1996; Pollastro et al., 2003). However, in most of the cases, no well data penetrate below the Ellenburger Group. Above the basement, unconformably lie the Cambrian rocks of Wilberns and Riley Formations (Denison, 1989). The Riley Formation consists of the oldest Hickory Sandstone Member, Cap Mountain Limestone Member, and the youngest Lion Mountain Sandstone Member, whereas, the Wilberns Formation is made up of (from oldest to youngest) the Welge Sandstone Member, Morgan Creek Limestone Member, Point Peak Member, and San Saba Limestone Member (Figure 2). These rocks were deposited in shallow marine environments, which were often subaerially exposed (Preston et al., 1996; Smith, 2004). Their thickness ranges from about few meters to 915 m (~3000 ft) in the south and southeast area near the LU

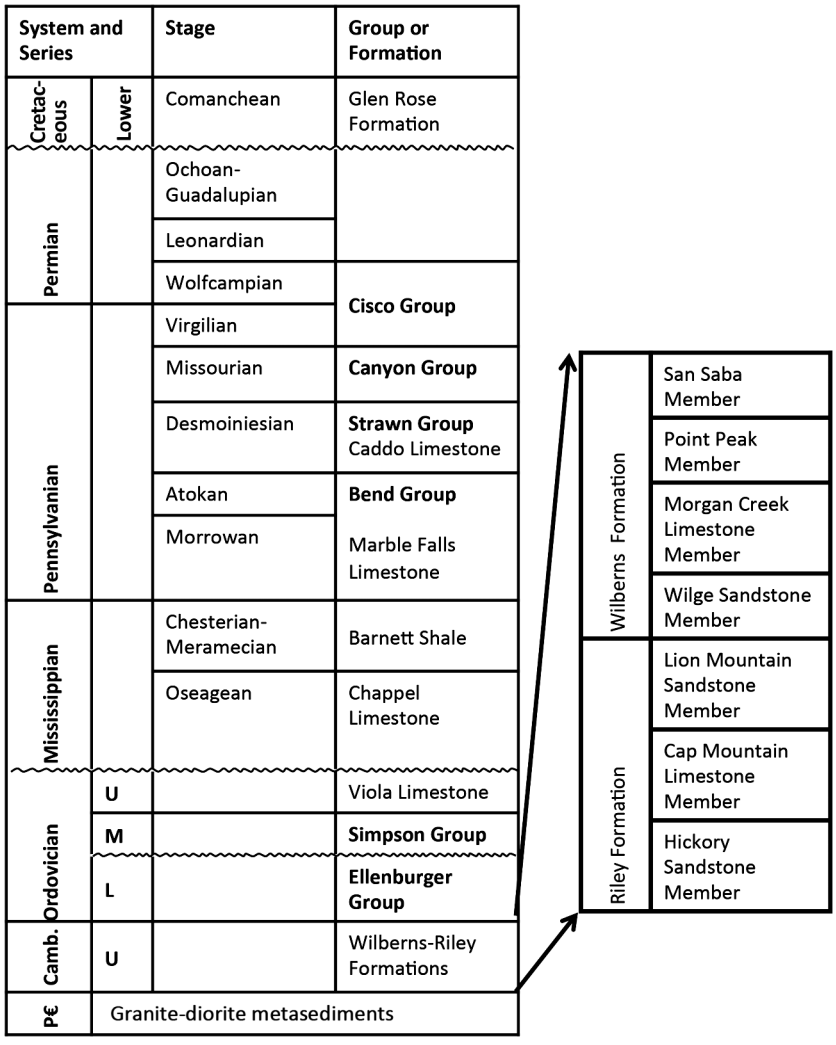

Figure 2. Generalized stratigraphic column in the FWB modified from Pollastro et al. (2003) and Smith (2004). The details of the Cambrian stratigraphy are based on the LU area, central Texas.

(Preston et al., 1996; Smith, 2004; Pollastro et al., 2007). The Cambro-Ordovician Ellenburger Group conformably overlay the Wilberns Formation. It predominantly consists of porous dolomite and limestone with abundant chert and occasional sandstone units. These rocks are characterized by numerous karst, solution-collapse, and brecciated structures (e.g., Loucks, 2003; Montgomery et al., 2005; Sullivan et al., 2006; Loucks and Ruppel, 2007; Dennie, 2010). In the central part of the FWB, basement faults have influenced the Ellenburger subaerial karst features, and these features have helped to reactivate the faults (Sullivan et al., 2006). Above the Ellenburger Group, the Middle and Upper Ordovician Simpson Group, Forrestberg Limestone, and Viola Limestone were deposited, but these units are absent on the southeast area (Bruner and Smosna, 2011). In the south and southeast area, the Mississippian Barnett Shale unconformably overlays the Cambro-Ordovician Ellenburger Group (Pollastro et al., 2003; Montgomery et al., 2005; Dennie, 2010; Bruner and Smosna, 2011). The absence of the Devonian and Silurian rocks indicates an erosional surface (unconformity) above the Ellenburger Group. The thickness of the Barnett Shale varies across the basin. It is as thick as 213 m (~700 ft) in the northeast corner, whereas the thickness decreases to about 9 m (~30 ft) in the south and southeast corner (Montgomery et al., 2005; Loucks and Ruppel, 2007; Bruner and Smosna, 2011). The Barnett Shale is overlain by the Mississippian Marble Falls Limestone, which in turn is covered with the Atokan conglomerate and sandstone (Bruner and Smosna, 2011). Above these Paleozoic units, lies a relatively thin cover of the Cretaceous and Quaternary sediments.

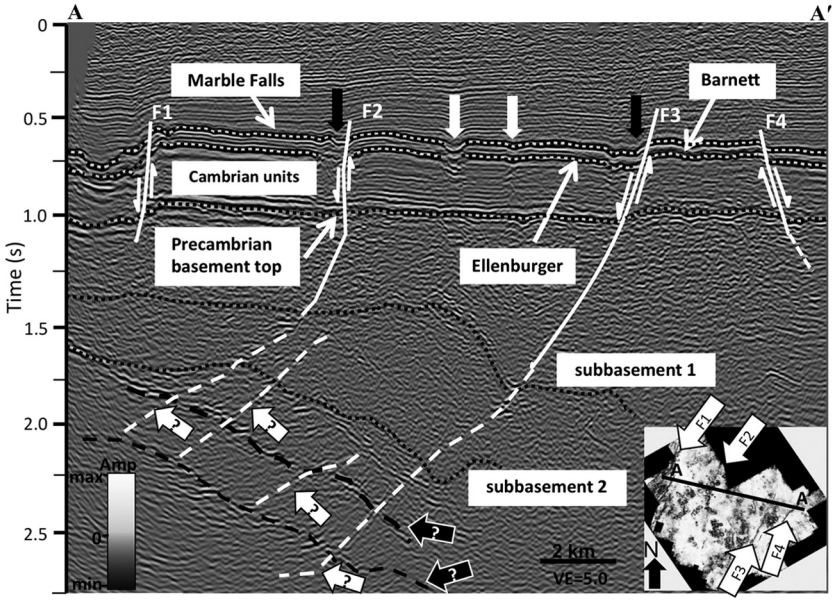

Figure 3. Interpreted seismic section across line AA′ as shown in the inset. Four major faults, namely, F1, F2, F3, and F4, were picked that align northeast–southwest with the regional trend of the OFTB. Major Paleozoic horizons, the top of the Precambrian basement, and two subbasement surfaces are picked (dotted black lines). The Paleozoic reflector such as the Ellenburger Group, Marble Falls Limestone, and Barnett Shale are shown. The Ellenburger Group shows many of the karst and collapse features. Some of these collapse features are related to the basement and basement faults as identified by the black arrows, whereas the others are not related and are shown by white arrows. Some unknown strong reflectors (dashed black line) below the basement are probably related to the intrusive bodies.

Geophysical data preparation, processing, and interpretation

In this study, we analyzed 3D seismic data, gravity, and aeromagnetic data and integrated the results with other geospatial data including well logs, geologic maps, fault maps, and digital elevation models (DEMs) to interpret the basement structures. In the following sections, we discuss the details of these methods, the basics of the processing techniques, and the interpretation.

Seismic data

3D seismic data preparation

The 3D seismic survey covered approximately 220 km^2 (~85 sq mi) and has 1189 inlines and 1119 crosslines with spacing of 16.76 m (~55 ft) each. We used the prestack, time-migrated seismic volume for interpretation purposes. The data processing was focused on imaging the shallow Barnett Shale objective, leaving some low-frequency migration artifacts in the deeper portion of the seismic data. In an ideal case, one should prestack depth migrate the data to image the basement. Here, we applied a bandpass Butterworth filter (10–15–24–30 Hz) to reduce the migration artifacts and higher band frequency related multiples. We picked some of the key Paleozoic horizons and faults along with some of the strongest subbasement reflectors (Figure 3). Given the flat nature of the Paleozoic section, these dipping reflectors represent geology of the area rather than multiples. These reflectors are discontinuous in places but are trackable. Below these strongest reflectors, there are various discontinuous and weaker reflectors. These reflectors truncate upward and terminate into the subbasement reflectors. These subbasement reflectors form bounding envelopes (Figure 3). We also mapped some of the major fault patterns, which exhibit north-northeast–south-southwest trends.

Another major technique applied to the seismic data was attribute analysis. Volumetric seismic attribute analysis not only helps to delineate and identify major structural features such as faults, karst, and collapse features, but also aids visualization of dip and azimuth variations and reflector rotation. The

volumetric attributes, such as amplitude variation, coherence, curvature, dip and azimuth variation, reflector rotation, and structurally oriented filters are routinely used in the 3D seismic interpretation (Brown, 1996; Chopra and Marfurt, 2005, 2007a, 2007b). We used an internally developed software package to generate numerous volumetric seismic attributes. Among them, coherence, curvature, reflectors rotation, and dip and azimuth variation of the reflectors were the most useful in this study. The results from the volumetric attributes analysis are shown in Figures 4–7. Discussion of the mathematical details and theoretical background of these methods is beyond the scope of this paper, with the details found in Brown (2011) and Chopra and Marfurt (2007a).

Seismic data interpretation

Although the seismic data cover only a small part of the study area, their spatial resolution helped to easily identify major subsurface features. We identified and mapped major faults, key Paleozoic horizons, the top of the Precambrian basement, and subbasement reflectors in the seismic volume. Figure 3 shows the main structural features observed in the seismic data on a representative vertical slice through the central portion of the survey. The top of the Precambrian basement is clear throughout the seismic volume. Above the basement, the Wilberns and Riley Formations were clear, and we mapped the Ellenburger Group and the Marble Falls Limestone horizons. The Barnett Shale lies between these units and thins from A toward A′ (eastward). Montgomery et al. (2005) and Bruner and Smosna (2011) discuss the absence of the Viola Limestone, Simpson Group, and the Forrestberg Limestone in the southern part of FWB. We can confirm this in the seismic section (Figure 3). Four major faults, namely, F1, F2, F3, F4, are mapped (Figure 3). These normal faults have a regional trend of north-northeast–south-southwest. Fault F1 is shallow but has the largest offset, which is about 0.25 s. Fault F2 has a small offset of a few milliseconds. We traced this fault to a depth of about 1.4 s. Fault F3 cuts across the Paleozoic sequences as well as the Precambrian basement. This fault can be trace down to about 1.5 s. Below this depth, it is faintly visible and is shown by a dashed white line in Figure 3. Deep in the seismic section, we observe other potential faults (dashed white lines). We suspect these features are probably normal and thrust faults that trend north-northeast from the eastern LU and are most likely related to faults associated with the Ouachita orogeny (e.g., Ferrill and Morris, 2008; Mosher et al., 2008; Levine and Mosher, 2010). Fault F4 has a smaller offset and is mapped to about 1.1 s. Below 1.3 s, we also picked some strong and continuous intrabasement reflectors (denoted as subbasement 1 and subbasement 2 in Figure 3). They are irregular, curved, and truncated in 3D perspective view. The irregular shapes, truncation, and curvature of the basement are the product of the complex history of Ouachita tectonics and multiphase uplift in the Llano area that is related to Grenville orogeny and subsequent erosional unconformity (e.g., Freeman and Wilde, 1964; Mosher et al., 2008; Levine and Mosher, 2010). At about 2.0 s and below, there are more intrabasement reflectors (dashed black lines in Fig 3). They are discontinuous through the seismic volume and hence are more difficult to pick. We interpret these events as possible intrusive bodies, sills, and dikes mostly related to the magmatism that is observed in the eastern LU and are probably related to the Grenville orogeny.

We used different volumetric attributes to aid the seismic interpretation process including curvature, coherence, combined dip and azimuth, and reflector rotation. Corendering these attributes and the seismic data together is a very useful technique to visualize subtle geologic features that may not be readily observed in the traditional seismic amplitude display. Coherence attributes measure the similarity of the neighboring seismic traces along the dip and azimuth of the seismic reflectors (Chopra and Marfurt, 2007a). This attribute is a useful tool to visualize faults, river channels, reefs, karst features, and collapse features. Curvature approximates local seismic reflectors with a quadratic surface and highlights folds, flexures along the fault planes, collapse, and karst features. Figure 4 shows a time slice

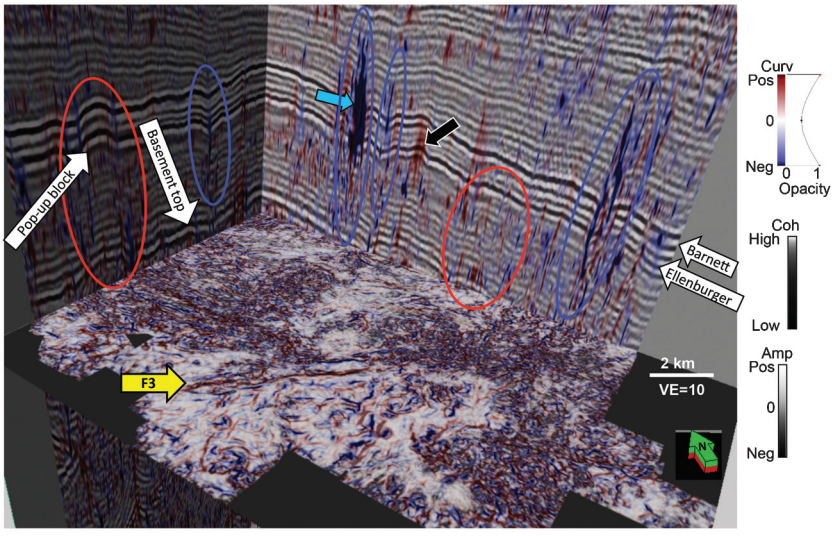

Figure 4. Illustration of geometric attributes using a 3D chair diagram showing vertical slices through the seismic amplitude and a time slice at 0.98 s (approximate basement) through coherence corendered with most-positive and negative principal curvature. Blue areas (such as indicated by the cyan arrow) highlight valleys and bowls, and red areas (such as indicated by the black arrow) highlight ridges and domes. Probable pop-up block is observed in the northwest corner of the survey indicating complex deformation history of the area.

through corendered coherence, most-positive and negative principal curvature near the approximate top of the Precambrian basement with a vertical slice through seismic amplitude corendered with the two curvatures. Blue areas (such as indicated by the cyan arrow) highlight valleys and bowls, and red areas (such as indicated by the white arrow) highlight ridges and domes. Some of these valleys and ridges cut across the Barnett Shale and Ellenburger Group and extend at least to the basement. Note the complex deformation of the basement that controls the collapse features in the shallower Ellenburger Group (such as the area indicated by the red and blue ellipse). In the northwest corner of the survey, we also observed a pop-up block throughout the Paleozoic sequences. This indicates the presence of transpressional tectonic setting, and the area has a complex deformation history. To find the vertical extent of karst and collapse features observed in the Marble Falls Limestone and Ellenburger Group, we analyzed corendered times slices of coherence, most-positive and negative principal curvature at different depth ranging from 0.75 to 1.1 s and plotted them against the seismic data (Figure 5). The slice at $t = 0.75$ s approximates the top of the Ellenburger Group where we see all of the picked faults F1, F2, F3, and F4 and significant numbers of the collapse and karst features (indicated by cyan arrows). We observe that some of these karst and collapse features align well with faults as in F2 and F3 forming a "string of pearls" as seen in other FWB surveys (Schuelke, 2011). At $t = 0.9$ s, these collapse and karst features are not clearly visible (except in the southwest corner). At this level, we are at one of the sandstone units of the Riley or the Wilberns Formation. At the $t = 1.0$ s time slice, some of these karst and collapse features (indicated by cyan arrows) reappear in the southeast corner of the survey. We interpret this time slice as cutting to one of the limestone members of the Riley or the Wilberns Formation. At $t = 1.1$ s, none of these karst or collapse features are visible. At this depth, we are looking into the Precambrian basement in the area, which is mainly composed of granite and diorites as shown in Figure 2 and reported by Smith (2004), Sullivan et al. (2006), and Bruner and Smosna (2011).

The combined dip and azimuth attributes help us identify and interpret the orientation of dipping seismic reflectors, faults, and folds. We corendered the combined dip and azimuth attribute and seismic amplitude values and show the result in Figure 6. Faults F1, F2, F3, and F4 are all observed with brighter (higher intensity/luminosity) color indicating steeper dips of about 15°–20°. Faults F1, F2, F3 are dipping toward the north–northwest, whereas F4 dips south–southeast. Reflector

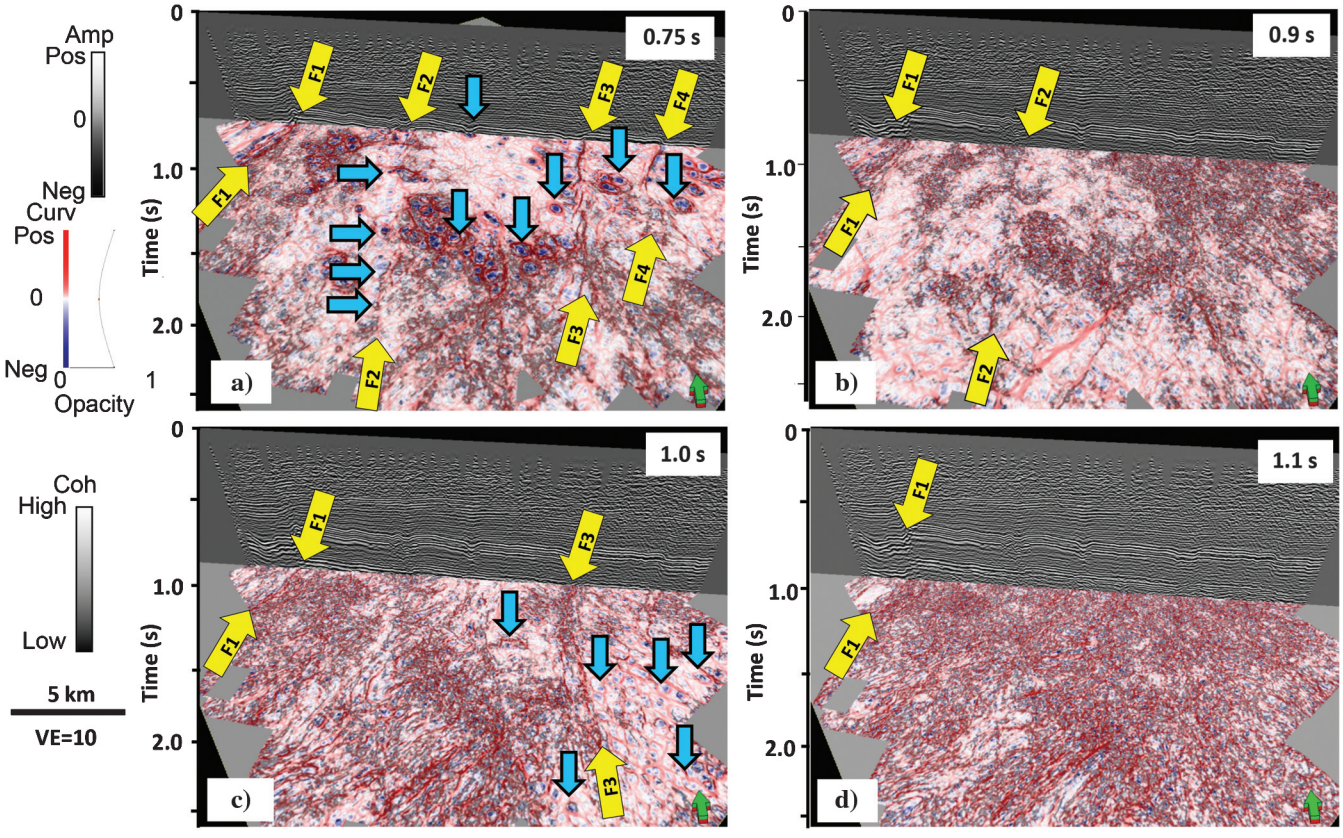

Figure 5. Display of karst, collapse features, and faults in the seismic data using coherence and curvature attributes and arbitrary seismic section at time: (a) $t = 0.75$ s, approximate Ellenburger top (b) $t = 0.9$ s, at a Cambrian Unit (c) $t = 1.0$ s, approximate basement top, and (d) $t = 1.1$ s in the basement. Cyan arrows indicate collapse features, whereas sets of yellow arrows show major faults mapped in the area.

rotation is a more recently introduced attribute (Marfurt and Rich, 2010) that estimates the nonquadratic features of the local surfaces. Mathematically, the mean curvature is the divergence of the vector dip and the reflector rotation is the curl of the reflector dip. At $t = 0.7$ s and $t = 1.0$ s, we observe strong north-northeast–south-southwest trending fabrics as shown in Figure 7a and 7b. These fabrics match well with the structural trend of the Balcones fault and the thrust faults of the OOB (Figure 1). We also observed possible Reidel shear (?) structures in between faults F1 and F2 (Figure 7a). The presence of these shear zones indicates the transpressional tectonic setting in the area during the Paleozoic. We also extracted vertical slices along the arbitrary lines AA′ and BB′ and show these seismic sections in Figure 7c and 7d. We identified key Paleozoic horizons and some of the Proterozoic reflectors. These subbasement Proterozoic reflectors are probably igneous sills and intrusions related to the Grenville orogeny similar to those observed in the nearby eastern LU (Carter, 1989; Mosher et al., 2008; Barker and Reed, 2010). There are some unidentified reflectors (marked by white block arrows; Figure 7c and 7d). We believe these reflectors are either faults related to the Ouachita orogeny or are some metasedimentary or metavolcanic Proterozoic horizons.

With the help of all these interpretations, we constructed the 3D perspective view of the time-structure map with the major basement structures, mapped faults, and key Precambrian horizons shown in Figure 8. The top of the Precambrian basement is relatively flat and continuous. The Proterozoic subbasement surfaces are irregular and truncated. These surfaces resemble the shape of intrusive igneous bodies such as sills or plutons. Faults F2 and F3 are deep seated and cut across the entire Proterozoic and Paleozoic sequences in the area, whereas faults F1 and F4 are shallow and are mapped in the Paleozoic sequences and in the shallower portion of the Precambrian basement.

Gravity and magnetic data

Gravity and magnetic data preparation and processing

The terrestrial gravity and aeromagnetic data for the continental United States are freely accessible online at Pan American Center for Earth and Environmental Studies (PACES, 1995). We downloaded the regional gravity and magnetic data for an area of about 2° out on each side of the seismic survey. One of our goals

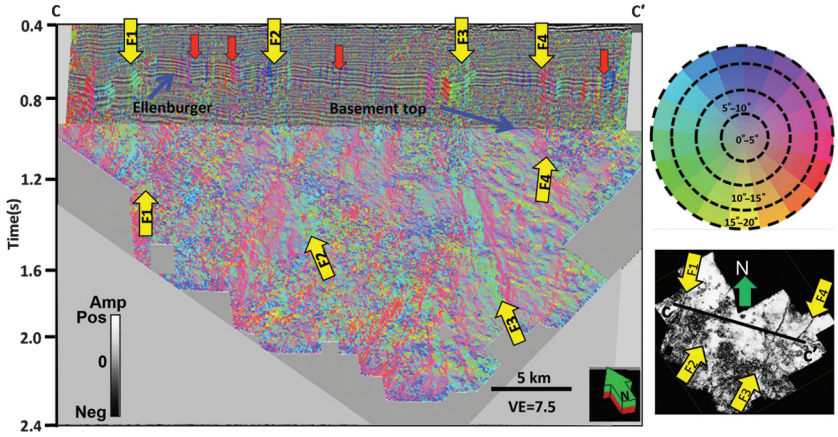

Figure 6. Combined dip and azimuth attributes corendered with arbitrary seismic section at line CC′ as shown in the inset with a time slice at 0.98 s. The brighter color represents a higher dip (the highest dip amount is 20°). Blue, red, yellow, and green colors represent structures dipping toward the north, east, south, and west, respectively. Faults F1, F2, and F3 are green and dip toward the west–northwest, whereas fault F4 is red and dips east–northeast. The red arrows represent vertical karst and collapse-related linear features that cut as deep as the top of Ellenburger Group.

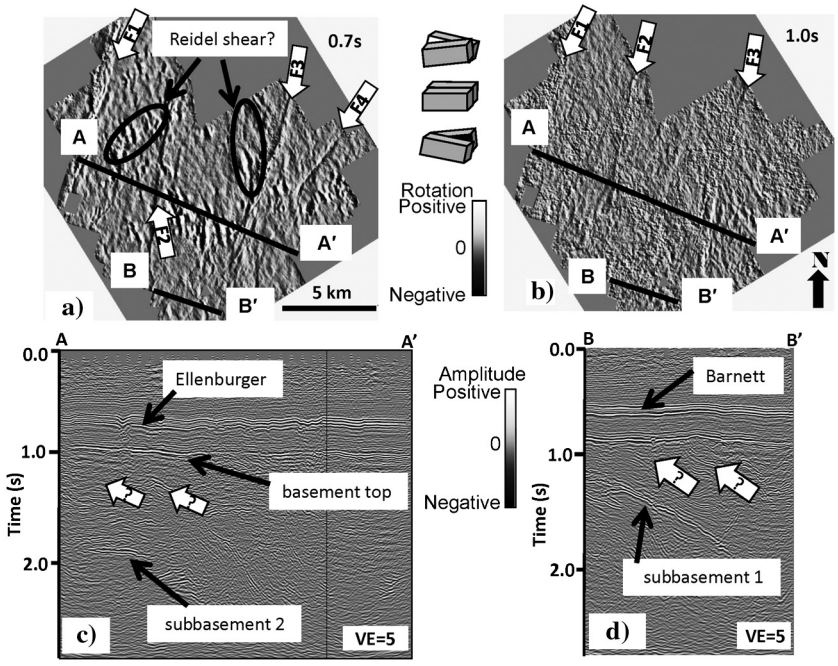

Figure 7. Time slice through the reflector rotation at (a) $t = 0.7$ s (approximate top of the Ellenburger) and (b) $t = 1$ s (approximate top of the basement) showing strong north-northeast–south-southwest trending fabrics. White lineaments are down to the right (clockwise rotation), and black lineaments are up to the right (counterclockwise rotation). Probable Reidel shear structures are observed at the top of the Ellenburger Group. (c and d) Vertical slices through seismic amplitude along lines AA′ and BB′. Key Paleozoic horizons and some strong Proterozoic reflectors are identified. Yet others are unidentified as shown by white arrows in (c and d).

is to determine if the regional potential field data relates the basement structures mapped on the seismic volume with the large-scale OOB, Lampasas arch, and the LU tectonic units in the study area. The regional data covers the area between 30° north to 34° north latitudes and 95° west to 99° west longitudes (Figures 1, 9, and 11). We used complete Bouguer anomaly (CBA) gravity values from the PACES database for further mapping and processing and used the Texas state magnetic data to analyze magnetic anomalies. These latter data were collected as part of the National Uranium Resource Evaluation (NURE) program in 1973 and is freely available online at the USGS Web site (Bankey, 2006). We used a 2 km (~6562 ft) grid spacing for CBA and total magnetic intensity (TMI) grids. We also reduced the TMI data to the magnetic north pole so that the resulting residual magnetic anomalies will lie directly above the magnetic source (Blakely, 1996) unless there is a strong remanent magnetization present. This reduced-to-pole residual TMI grid was used for further processing and filtering the magnetic data. Geosoft software was used for processing and analyzing the potential field data.

To enhance the visualization of gravity and magnetic anomalies, their shapes, and boundaries, we used various wavelength filters. We applied an upward continuation filter to the CBA to estimate the regional anomalies and subtracted the result from the CBA map to obtain a residual CBA map (Figure 9a). We also applied the directional derivative, tilt derivative, and total horizontal derivative filters to the gravity and magnetic data to delineate boundaries of intrusive bodies, faults, and other lateral

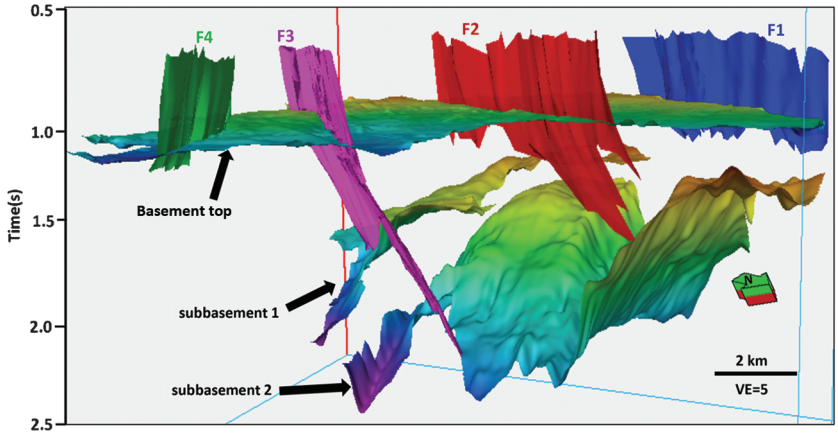

Figure 8. A 3D perspective view of the picked faults and horizons on the seismic data. F1, F2, F3, and F4 are the major faults mapped. These faults have northeast–southwest trends with F1, F2, and F3 dipping northwest, whereas F4 dips southeast. The top of the basement is at about $t = 1.0$ s. These basement and subbasement surfaces represent different tectonic stages in the area.

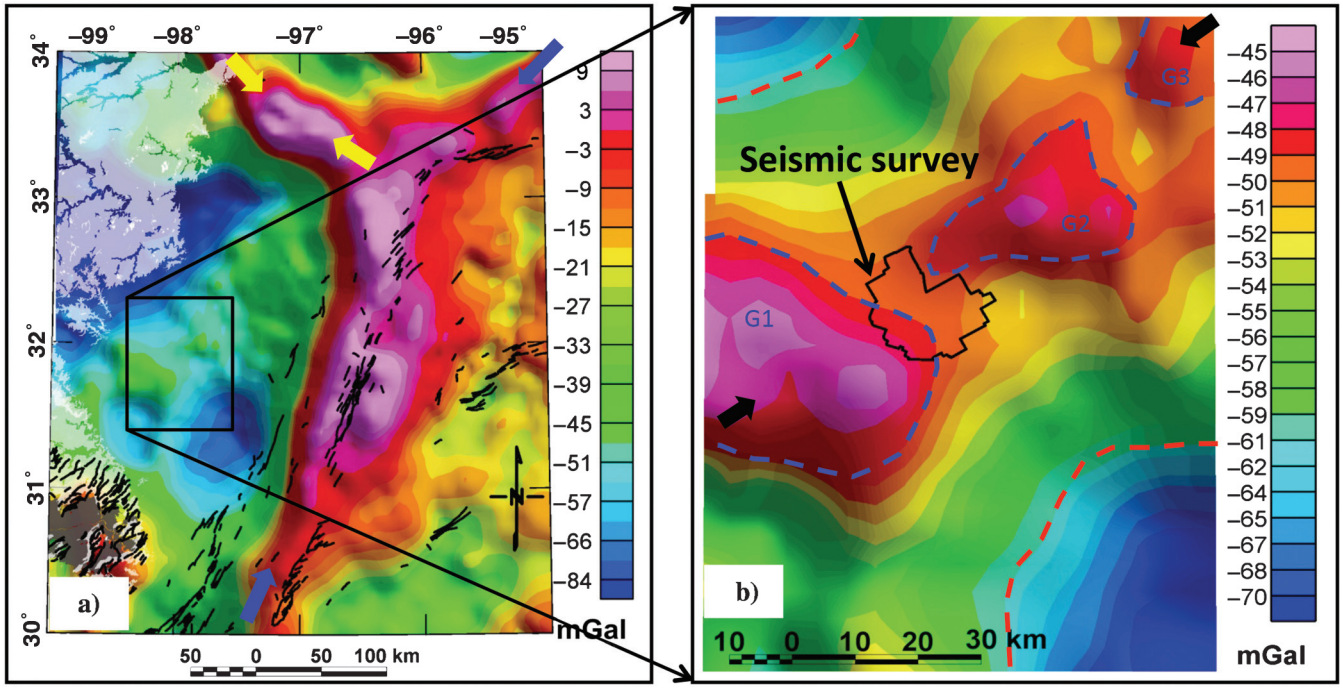

Figure 9. CBA maps of the study area. The set of blue and yellow arrows (a) represents gravity highs related to the OOB and SOA, respectively, whereas the gravity high in the southeast corner is related to the LU. The FWB is partly associated with a regional gravity low. Black lines represent surface faults (>4 km). Gray and white areas in the western side show Proterozoic and Paleozoic rock exposures, respectively. (b) Magnified view showing a series of northeast–southwest-trending local gravity high anomalies, namely, G1, G2, and G3, shown by a set of black arrows.

changes using edge detection techniques. Discussions of the mathematical and theoretical details of these filters are found in Miller and Singh (1994), Blakely (1996), and Verduzco et al. (2004).

In addition to the wavelength and edge-detecting filters, we also applied Euler deconvolution techniques to the magnetic data to determine the depth to the basement of the magnetic anomalies. The Euler deconvolution method relates the vertical and horizontal gradients of the residual TMI values with help of geometry of the magnetic bodies given by the structural index (SI) (e.g., Thompson, 1982; Barbosa et al., 1999). In addition to estimating basement depth, solutions obtained from the Euler deconvolution help to delineate source geometry and boundaries and can map a fault if the proper SI value is used for the given fault offset depth and the location of the fault. Shallow faults with larger offsets and irregular contacts are assigned an SI value of 0, whereas deeper faults with small offsets are assigned an SI value of 1 (Reid et al., 1990). Although the solution form Euler deconvolution techniques helps us to locate the anomaly of isolated magnetic bodies with the appropriate SI, solutions in areas with multiple source and complex geometry can be problematic (Blakely, 1996). In this paper, we used SI values of 0 to map deeper faults and 0.5 and 1 to map the top of the Precambrian basement.

Interpretation of gravity and magnetic data

In a study such as this, potential field data such as gravity and magnetic surveys have lower spatial resolution than seismic reflection data. However, they are very helpful for understanding regional geologic and tectonic settings of the area. The CBA anomaly in the area varies by about 100 mGal. We observed major tectonic units surrounding the FWB such as the LU, OOB, and SOA, which are associated with regional gravity highs. A prominent gravity low is associated with the FWB basin. We focused on the local area that contains the seismic data and analyzed gravity features (Figure 9b). The seismic survey area lies within a series of local gravity high anomalies (G1, G2, G3; marked by dashed blue polygons, Figure 9b) with a northeast–southwest regional trend. Two major gravity lows lie to the northwest and southeast sides of these features (marked by dashed red polygons).

To aid in the interpretation, a residual gravity anomaly map was constructed by subtracting the surface resulting from upward continuing the data to 40 km (Figure 10). Major tectonic units are identified on this map, including the approximate boundaries of the FWB, LU, SOA, and OOB interior zone. Inside the FWB, two major gravity lows are observed. To the northwest, a large linear gravity minimum is known as Abilene gravity minimums (AGMs). Adams and Keller (1996) interpret its source to be potentially a Precambrian granitic batholith that is similar to the size of Sierra Nevada batholith. Northeast of the LU, another gravity minimum (G4) of similar intensity of the AGM but of smaller extent is observed. We interpret this minimum as similar to that of the AGM in its origin. We hypothesize that the encroaching Ouachita frontal thrust in the Late Paleozoic played an important role in creating elliptical shape of the gravity minimum (G4), with its longer axis parallel to the direction of the Ouachita frontal thrust zone. The analogy can be drawn from the Sudbury Structure, Ontario, Canada, where the impact structure was intensely deformed by the Grenville orogeny (Boerner et al., 2000).

We also analyzed the magnetic data and a reduced-to-pole residual TMI map is shown in Figure 11. Magnetic highs related to the OOB and SOA are observed (shown by sets of white and yellow arrows, respectively; Figure 11a) Within the FWB itself, there are several magnetic bodies giving rise to interfering anomalies. The localized TMI map with a focus on the seismic survey area is shown in Figure 11b. Two positive local magnetic anomalies (M1 and M2) are observed in the vicinity of the seismic survey. These anomalies are related to the folded and bulged structures (subbasement 1 and subbasement 2) shown in Figures 3 and 8, which we interpret to be igneous intrusions related to the eastern LU. We also observe a local magnetic minimum, M3 in the residual TMI map. This minimum is partly related to the thicker Cambrian sediments to the northeast side of the LU (Preston et al., 1996; Smith, 2004) and probably partly due to the felsic intrusive bodies from the Grenville orogeny (Carter,

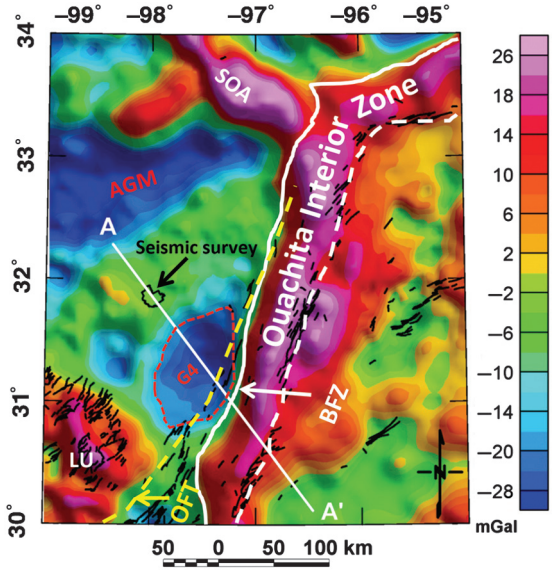

Figure 10. Residual CBA map of the study area after applying a 40-km upward continuation filter. Major tectonic units and its boundaries are tentatively drawn based on the observed gravity anomaly. The acronyms used are as follows: AGM = Abilene gravity minima, BFZ = Balcones fault zones, LU = Llano uplift, OFT = Ouachita frontal thrust, and SOA = Southern Oklahoma aulacogen. AA′ is a modeled gravity profile across the OOB (Figure 12). We tentatively draw the OFT (dotted yellow) line based on work by Kruger and Keller (1986) and Flawn et al. (1961).

1989; Mosher et al., 2008; Barker and Reed, 2010; Levine and Mosher, 2010).

We modeled a 272-km (~169 mi)-long residual CBA gravity profile AA′ (Figure 10) across the OOB using seismic, drilling, and geologic data as constraints. The density model along the profile is shown in Figure 12. We chose this profile in such a way that it crosses the 3D seismic data and the most important tectonic units in the area. A few of the interpreted well logs lie in the profile, but none penetrate through the shallow Ellenburger Group. The average Moho depth in the area has been estimated to be about 40 km (e.g., Kruger and Keller, 1986; Keller et al., 1989; Gao et al., 2008). Based on this model, we interpret the Moho depth to range from about 42 km in the FWB to about 37 km in the GCP. The mantle and the lower crust were assigned typical average densities of 3.3 and 3.0 g/cm^3, respectively. At about 3 km depth, we modeled shallow igneous body with density of 2.65 g/cm^3, which we interpret to be a granitic sill. A prominent local gravity minimum (G4) is located at the center of the profile (Figure 10). Some researchers have interpreted G4 to be related to thick sedimentary units of the FWB. This contradicts the well log data, which show the top of the Ellenburger Formation in this area is rather flat (Montgomery et al., 2005; Bruner and Smosna, 2011). To model the gravity low of G4, we took an alternative modeling approach by thickening the Cambrian units of Riley and Wilberns Formation to some extent (Preston et al., 1996) and emplacing a low-density (2.6 g/cm^3) granitic batholith in the upper crust. The density variation for granite at the given depth is as Oliver (1977) suggests for the Sierra Nevada granites. We used seismic data, well logs, and geospatial database to constrain the upper few kilometers of the model. To determine the densities of the Paleozoic units from the seismic data, we used Gardner's empirical relation (Gardner et al., 1974) between the density and P-wave velocity. We compared and confirmed these densities with the aid of well log in the area. In the FWB, the top of the Precambrian basement is at the depth of about 2.5–3.5 km (~8000–11500 ft.), whereas the depth of the Cambrian unit ranges between 1.4–1.8 km (~4500–5800 ft.). The Ellenburger Group overlies the Cambrian units. The top of the Ellenburger Group is relatively flat and is overlain by the Barnett shale and Marble Falls Limestone. Cretaceous and Quaternary sediments unconformably overlie the Paleozoic sequence. To the southeast side of G4, lies the OOB. We modeled the Ouachita frontal zone and Ouachita interior zones with densities of 2.64 and 2.71 g/cm^3. The difference in densities is based on the rock types they contain. The frontal zone mostly consists of preorogenic off-shelf and synorogenic deep-water rocks, whereas the interior zone mostly contains metamorphosed rocks from of the interior metamorphic belt (Viele, 1989). Our model suggests that the root of the OOB is as deep as 10 km and deepens southward, which matches other estimates for the area (Kruger and Keller, 1986; Arbenz, 1989; Keller et al.,

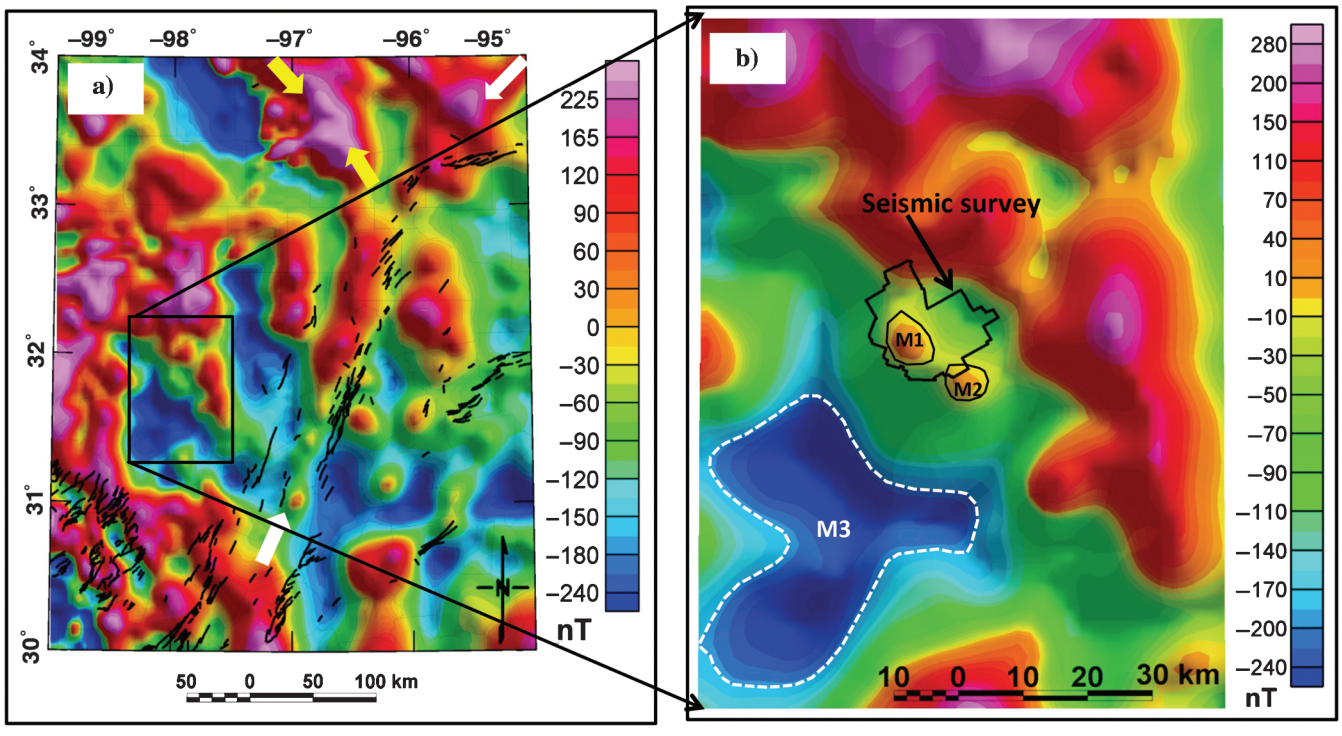

Figure 11. Residual TMI maps of the study area after reducing to magnetic pole. (a) Residual TMI map of the regional area. The set of white and yellow arrows represents magnetic highs related to the OOB and SOA, respectively. Black lines represent surface faults (>4 km). (b) Magnification with outlines of the major magnetic anomalies in the vicinity of the seismic survey.

1989). Under the OOB, a mafic intrusion was also included to model prominent gravity high and may mark the Cambrian margin of North America as is indicated further to the east by Keller et al. (1989) and Mickus and Keller (1992). Further to the south lies the GCP. The magnetic anomalies across the profile are complex due to presence of the multiple magnetic sources in the basement of the area and the uncertainty of the remnant magnetization values. For this reason, we did not model magnetic data. However, we compare the gravity and magnetic anomalies along profile A – A′ (Figure 12).

To extend our mapping of the top of the basement beyond the seismic survey, we performed Euler deconvolution on the reduced-to-pole residual TMI data. The results of the standard Euler solutions obtained are shown in Figures 13–15. In Figure 13a, we show the standard Euler solution computed with a SI of 0 and a tolerance error less than 12% plotted on top of the reduced-to-pole TMI map. The solutions clustered around the magnetic anomalies. Next, we generated a depth to the top of basement map (Figure 13b) of the area using the solutions obtained from Figure 13a and compared these two maps. The top to the magnetic basement ranges from about 400 to 5300 m (~1250–17,000 ft). The sets of the block arrows with same colors are used in both maps (Figure 13a and 13b). The positive and negative magnetic anomalies from Figure 13a are related to the deeper and shallower depth to the top of basement on Figure 13b, respectively, as shown by the black arrows. However, the area shown by the white arrow shows the opposite result with positive magnetic high anomaly related to shallower top of the basement. The depth to the top of magnetic basement within the seismic survey ranges from about 1500 to 2800 m (~5000–9100 ft). This basement depth interpretation lies within the error range of Euler deconvolution of magnetic data compared to the result from the seismic data.

Next, we plotted the Euler solutions on the filtered magnetic maps. Figure 14a and 14b shows the standard Euler solutions plotted on the tilt derivative and total horizontal derivative of reduced-to-pole residual TMI maps, respectively. The solutions are clustered along the edges of the magnetic anomalies on the tilt derivative maps where the zero values of the anomalies are observed. In Figure 14b, the Euler solutions are clustered at the center of the magnetic anomalies. Verduzco et al. (2004) and Lahti and Karinen (2010) explain that the tilt derivative has its zero values close to the edges of the magnetic bodies. In the case of total horizontal derivatives, the maxima are generally sharper and are directly above the edges of the anomalies.

We also compared the faults mapped in seismic data with the results from the Euler solution to see if they correlate. The results are presented in Figure 15. Figure 15b and 15c shows windowed Euler solutions with an SI of 0 and 1, respectively with a tolerance error of 12%. The trend and location of mapped faults F1 and F3 in Figure 15a matches with the location of these faults in Figure 15b and 15c, respectively. From the seismic section, we know that F1 is a large offset irregular fault, whereas fault F3 is a smaller offset planar fault suggesting the use of SI values of 0 and 1, respectively, as explained. However, the standard Euler solutions do

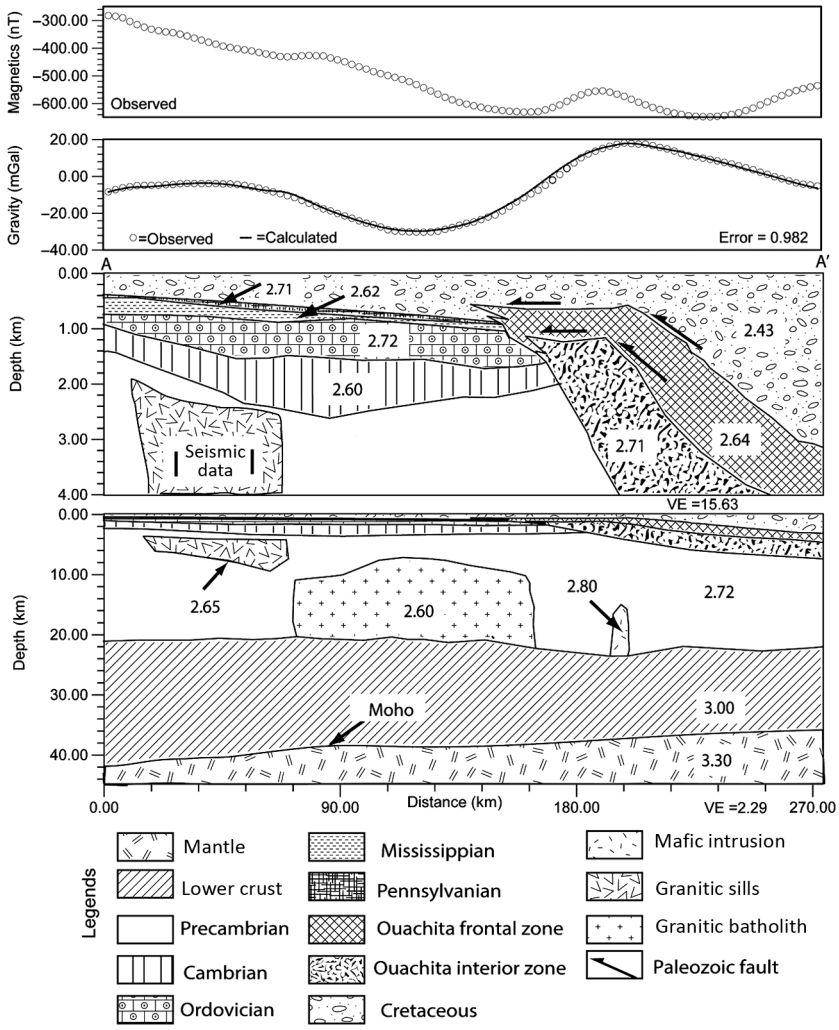

Figure 12. Regional gravity model across the OOB on profile AA′ across the seismic survey as shown in Figure 10 starting at FWB to the Gulf coastal plains. We used shallow well logs, seismic data, geospatial data, and geologic information from published literature to model the residual gravity. The density values are in g/cm^3. VE in the figure stands for vertical exaggeration showing that the third and fourth panels have different vertical scales.

not capture faults F2 and F4 that were mapped in the seismic section. We explain this by either the inadequate fault offsets or due to the insufficient difference in the magnetic sources across these faults.

Geologic and geospatial database

In addition to the seismic, gravity, and magnetic data, we also considered information obtained from other sources such as geologic maps, tectonic maps, fault databases, DEM data, interpreted well logs, and interpreted 2D deep seismic refraction profiles to generate a regional gravity model (Figure 11). The geologic maps, DEM data, and fault map are available online in the USGS Web sites. Well locations and digital well log data are accessible at no cost for download via the Texas Railroad Commission Website (Railroad Commission of

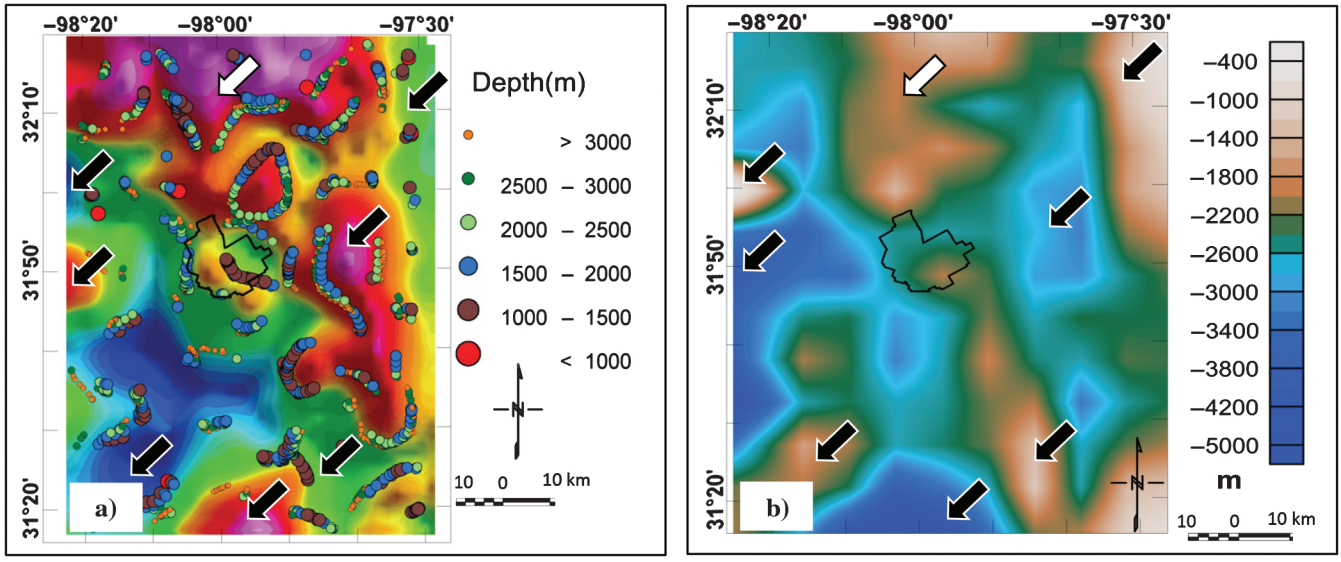

Figure 13. Depth to basement solution derived from Euler deconvolution with the SI value of 0. Reduced-to-pole residual TMI grid is used on to compute the solutions. (a) Standard Euler depth solutions on top of the reduced-to-pole residual TMI grid. (b) Contour depth map based on the solutions from (a). Sets of black and white arrows show relationships between basement depth and the magnetic anomalies, where black arrows show the area with inverse relation and white arrow shows the area with direct relation.

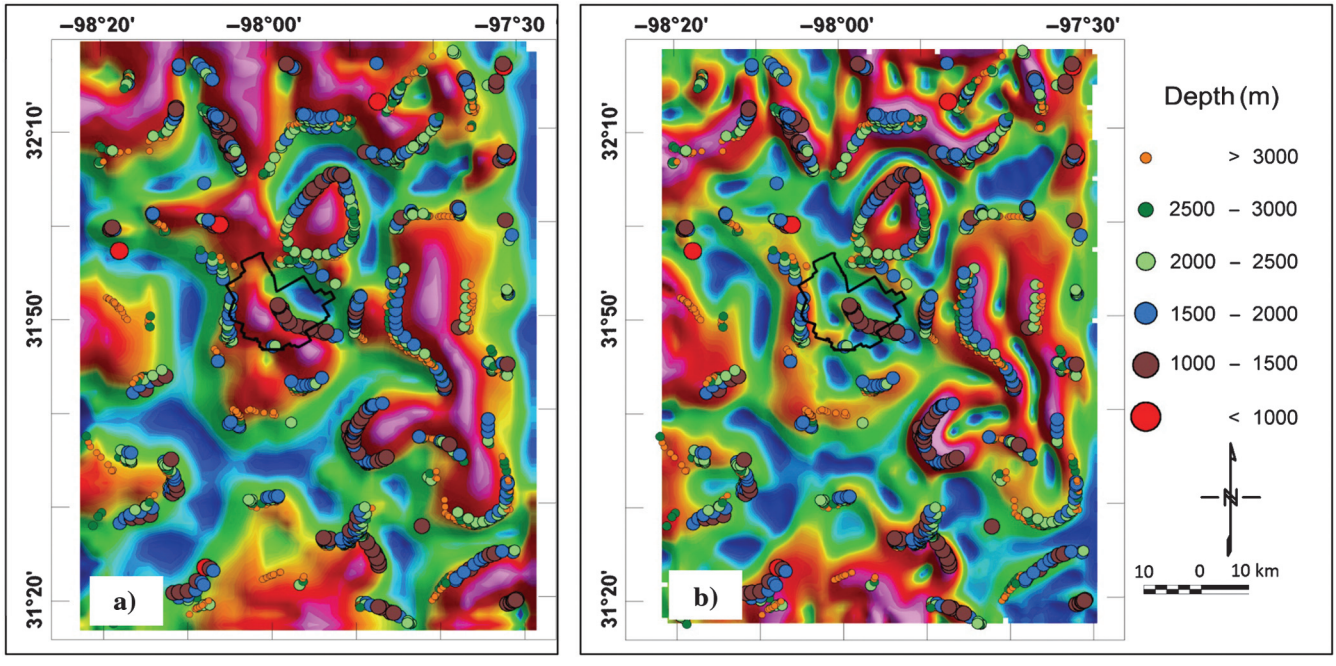

Figure 14. Standard Euler solutions from Figure 13 are plotted on top of (a) the tilt derivative and (b) the total horizontal derivative of the reduced-to-pole residual TMI map. The solutions are clustered around the edges (close to zero) and the center of the magnetic anomalies in (a, b), respectively.

Texas, 2010). All these data have been integrated to aid our interpretation of the geologic structure and tectonic setting of the southeast FWB region.

Integrated discussion of the results

After analyzing the seismic, gravity, magnetic, and geospatial data, we integrated these results and placed them in a tectonic context. We divide the tectonic evolution of the southeast FWB and its surrounding into following two broad categories.

The Proterozoic evolution

From the rocks exposed in the core of LU area and eastern LU, we now know that there existed a Mesoproterozoic terrane and orogenic belt along the southern margin of Laurentia during the Grenville orogeny (Mosher et al., 2008). During this orogeny, the southern margin of the Laurentia collided with an oceanic arc that was followed by the continental-continental collision, crustal thickening, and uplift (Mosher et al., 2008; Barker and Reed, 2010). During these processes, metamorphism and considerable magmatic activity took place, and granitic batholiths, sills and dykes were emplaced in the area. We observed some of these Precambrian subbasement reflectors in the deeper section of our seismic data as shown in Figures 3, 7, and 8. We relate these reflectors to the granitic intrusions or some of the metamorphosed units that resulted from these events. Our integrated gravity model (Figure 12) also includes batholiths and sills in the middle crust.

During the Neoproterozoic and Early Cambrian, the Rodinian supercontinent broke up to form a shallow-marine, passive margin that the OOB approximately followed and where the shallow marine and continental shelf deposits took place (Arbenz, 1989; Viele and Thomas, 1989). Extensional basins formed along the passive margin during this time. The shallow continental margin was bounded by oceanic crust until the Late Paleozoic (e.g., Keller et al., 1989). From exposures in the Ouachita Mountains and Marathon uplift and subsurface data, we know that preorogenic Ouachita strata were deposited during the Late Proterozoic–Early

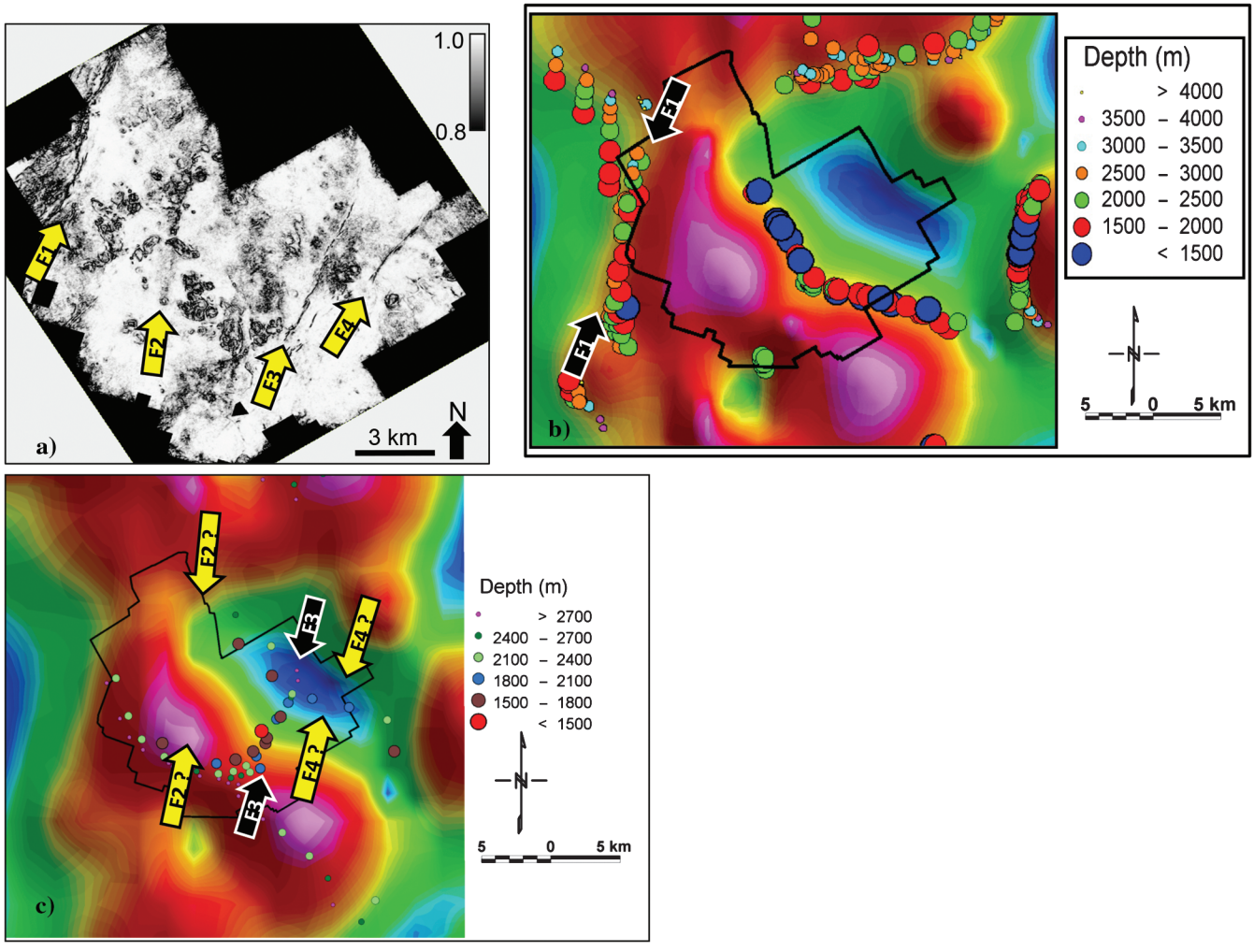

Figure 15. Comparing fault locations between seismic data and Euler solutions. (a) Faults F1, F2, F3, and F4 picked on 3D seismic data with coherence time slice at 0.75 s. (b and c) Windowed standard Euler solutions with SI values of 0 and 1. The trend and location of faults F1 and F3 from (a) tentatively match with the faults in (b and c), respectively.

Paleozoic and depositional environments ranged from deep-water to continental shelf to the shallow marine environment (Viele and Thomas, 1989). The preorogenic rocks include shale, sandstone, cherts, limestone, and dolomites. These rocks are identified as the lower unit of Ouachita facies. We included these units in the gravity model (Figure 12) with appropriate rock densities.

The Paleozoic and Mesozoic evolution

During the Cambrian, the whole area was still under a shallow ocean, when the Wilberns and Riley Formation were deposited as sandstone, shale, and limestone. The area was often subaerially exposed and sometimes submerged (Preston et al., 1996), and hence, we see karst and collapse features in the Cambrian units on the seismic data (Figures 4 and 5). In the Ordovician, carbonate rocks such as Ellenburger, Viola, and Simpson Groups were deposited. The presence of karst and collapse features in the seismic data (Figures 3–7) indicates its subaerial exposure during this time as well. During the Late Mississippian and Early Pennsylvanian, compressional tectonics started and the ocean closed. Inboard from this tectonic activity, the Barnett Shale with frequent limestone layers was deposited during this period. Early Pennsylvanian synorogenic deposits formed in the Ouachita frontal zone in a deltaic environment (Walper, 1982; Viele, 1989). Meanwhile, regional metamorphism occurred in the preorogenic Ouachita facies. The postorogenic Late Pennsylvanian Units (Strawn, Canyon, and Cisco Groups) are predominantly shale, sandstone, conglomerate, and red beds, which indicates a fluvial depositional system. The seismic section and analyzed seismic attributes (Figures 3–8) show these strata. The metamorphosed interior zone of the OOB is associated with regional gravity and magnetic high anomalies as shown in Figures 9–15.

The orogenic activity continued into the Early Permian forming the foreland FWB. Due to north–northwestward compression, the Bend arch, Muenster arch, and Lampasas arch formed around the FWB. We interpret faults F3 and F4 to bound a structural high related to the Lampasas arch (Figures 3, 5a, and 8). Many of the normal and reverse faults were active during the postorogenic phase. Most of these faults are buried, but they can be mapped in the seismic data (Figures 3–8). We also mapped some of these faults with help of the Euler deconvolution of magnetic data (Figure 15). The general trends of these faults match with the principal stress direction of the area during the Ouachita orogeny. Some of these faults such as F2 and F3 cut across the entire Paleozoic section and Precambrian basement (Figures 3, 6, 7, and 8) and the karst and collapse features observed in the Paleozoic sequences align along these faults (Figures 3–5). Elebiju et al. (2010) suggest the reactivation of some of the faults in the northeast portion of the FWB during the Ouachita orogeny, but we do not see the sign of reactivation of these faults in the southeast FWB. However, the presence of a pop-up block (Figure 4) and possible Reidel shear zones (Figure 7a) in the Paleozoic sequences of the southern FWB indicates the presence of transpressional tectonics in the area. The alignment of the collapse features with the mapped faults (Figures 4–7) suggests that there is some basement control on the overlying Paleozoic sequences and the associated reservoirs.

Conclusions

Although the basement and subbasement reflectors are visible in the seismic sections, they are hard to trace throughout the seismic volume. To improve the visibility of these reflectors, we used volumetric seismic attributes. Some of the basement and intrabasement reflectors are dipping and folded. We interpret the intrabasement reflectors in the southeast FWB to represent igneous intrusions. The gravity and magnetic maps and models agree with these interpretations. The solutions from Euler deconvolution for determining the top to the magnetic basement provided some useful results and validated the fault interpretation from the seismic data. Some of the normal and reverse faults that cut across the Paleozoic sequence are also visible and penetrate the basement. The observation of the pop-up block and the possible Reidel shear zones within the seismic survey area indicates the presence of transpressional stress and complex tectonic deformation of the southeast FWB. Karst features that were previously mapped in the northern part of the FWB are also present in the shallower section in the southeast FWB. Alignment of these karst and collapse features with the mapped faults indicates that the deep-seated faults and the collapse features are associated with reservoirs of the Ellenburger Group, Barnett Shale, and the Marble Falls Limestone.

Acknowledgments

Many thanks go to Marathon Oil Company for providing us a license to use their seismic data. The U.S. Geological Survey and Pan American Center for Environmental Studies (PACES) have made the gravity and magnetic data available to the public, and they can be accessed at http://research.utep.edu/paces/ and http://pubs.usgs.gov/ds/2006/232/. Seismic interpretation was done using Petrel Software using a license provided to University of Oklahoma (OU) for research and education purpose by Schlumberger. Attributes were generated using software developed by OU's AASPI industrial consortium. We would also like to thank N. Gupta and A. Roy for their help in effectively using the technology.

References

Adams, D. C., and G. R. Keller, 1996, Precambrian basement geology of the Permian basin region of West Texas and eastern New Mexico: A geophysical perspective: AAPG Bulletin, **80**, 410–431.

Aktepe, S., K. J. Marfurt, and R. Perez, 2008, Attribute expression of basement faulting-time versus depth migration: The Leading Edge, **27**, 360–367, doi: 10.1190/1.2896627.

Arbenz, K. J., 1989, Ouachita thrust belt and Arkoma basin: *in* R. D. Hatcher, Jr., W. A. Thomas, and G. W. Viele, eds., The Appalachian-Ouachita orogen in the United States, Geology of North America: F-2, Geological Society of America, 621–634.

Arbenz, K. J., 2008, Structural framework of the Ouachita Mountains, *in* N. H. Suneson, ed., Stratigraphic and structural evolution of the Ouachita Mountains and Arkoma basin, southern Oklahoma and west-central Arkansas: Applications to petroleum exploration: 2004 Field Symposium: Oklahoma Geological Survey, Circular 112A, the Arbenz-Misch/Oles volume, 1–40.

Bankey, V., 2006, Texas magnetic and gravity maps and data: A website for distribution of data, http://pubs.usgs.gov/ds/2006/232/, accessed 17 May 2011.

Barbosa, V. C. F., J. B. C. Silva, and W. E. Medeiros, 1999, Stability analysis and improvement of structural index estimation in Euler deconvolution: Geophysics, **64**, 48–60, doi: 10.1190/1.1444529.

Barker, D. S., and R. M. Reed, 2010, Proterozoic granites of the Llano Uplift, Texas: A collision-related suite containing rapakivi and topaz granites: GSA Bulletin, **122**, 253–264, doi: 10.1130/B26451.1.

Blakely, R. J., 1996, Potential theory in gravity and magnetic applications: Cambridge University Press.

Boerner, D. E., B. Milkereit, and A. Davidson, 2000, Geosciences impact: A synthesis of studies of the Sudbury structure: Canadian Journal of Earth Sciences, **37**, 477–501, doi: 10.1139/e99-062.

Brown, A. R., 1996, Seismic attributes and their classification: The Leading Edge, **15**, 1090, doi: 10.1190/1.1437208.

Brown, A. R., 2011, Interpretation of three-dimensional seismic data, 6th ed.: American Association of Petroleum Geologists, AAPG Memoir/SEG Investigations in Geophysics.

Bruner, K. R., and R. Smosna, 2011, A comparative study of the Mississippian Barnett Shale, Fort Worth basin, and Devonian Marcellus Shale, Appalachian basin: US Department of Energy, National Energy Technology Laboratory, report, DOE/NETL-2011/1478.

Carter, K. E., 1989, Grenville orogenic affinities in the Red Mountain area, Llano Uplift, Texas: Canadian Journal of Earth Sciences, **26**, 1124–1135, doi: 10.1139/e89-096.

Chopra, S., and K. J. Marfurt, 2005, Seismic attributes — A historical perspective: Geophysics, **70**, no. 5, 3SO–28SO, doi: 10.1190/1.2098670.

Chopra, S., and K. J. Marfurt, 2007a, Seismic attributes for prospect identification and reservoir characterization: SEG, Geophysical Development Series, no. 11.

Chopra, S., and K. J. Marfurt, 2007b, Volumetric curvature attributes add value to 3D seismic data interpretation: The Leading Edge, **26**, 856–867, doi: 10.1190/1.2756864.

Dalziel, I. W. D., L. H. Dalla Salda, and L. M. Gahagan, 1994, Paleozoic Laurentia-Gondwana interaction and the origin of the Appalachian-Andean mountain system: GSA Bulletin, **106**, 243–252, doi: 10.1130/0016-7606(1994)106<0243:PLGIAT>2.3.CO;2.

Denison, R., 1989, Foreland structure adjacent to the Ouachita foldbelt, *in* R.D. Hatcher, Jr., W. A. Thomas, and G.W. Viele, eds., The Appalachian-Ouachita orogen in the United States, Geology of North America: F-2, Geological Society of America, 681–688.

Dennie, D. P., 2010, An integrated paleomagnetic and diagenetic investigation of the Barnett Shale and underlying Ellenburger Group carbonates, Fort Worth basin, Texas: Ph.D. dissertation, University of Oklahoma.

Elebiju, O. O., G. R. Keller, and K. J. Marfurt, 2010, Case history investigation of links between Precambrian basement structure and Paleozoic strata in the Fort Worth basin, Texas, USA, using high-resolution aeromagnetic, HRAM data and seismic attributes: Geophysics, **75**, no. 4, B157–B168, doi: 10.1190/1.3435939.

Erlich, R., and J. Coleman, 2005, Drowning of the Upper Marble Falls carbonate platform (Pennsylvanian), central Texas: A case of conflicting "signals?": Sedimentary Geology, **175**, 479–499, doi: 10.1016/j.sedgeo.2004.12.017.

Ewing, T. E., R. T. Budnik, J. T. Ames, D. M. Ridner, and R. Dillon, 1990, Tectonic map of Texas: Bureau of Economic Geology: University of Texas at Austin.

Ferrill, D. A., and A. P. Morris, 2008, Fault zone deformation controlled by carbonate mechanical stratigraphy, Balcones fault system, Texas: AAPG Bulletin, **92**, 359–380, doi: 10.1306/10290707066.

Flawn, P. T., A. Goldstein, P. B. King, and C. E. Weaver, 1961, The Ouachita System: University of Texas, Bureau of Economic Geology.

Freeman, T., and G. Wilde, 1964, Age and stratigraphic implications of major faults in the Llano region, central Texas: AAPG Bulletin, **48**, 714–718.

Gao, S. S., K. H. Liu, R. J. Stern, G. R. Keller, J. P. Hogan, J. Pulliam, and E. Y. Anthony, 2008, Characteristics of mantle fabrics beneath the south-central United States: Constraints from shear-wave splitting measurements: Geosphere, **4**, 411–417, doi: 10.1130/GES00159.1.

Gardner, G., L. Gardner, and A. Gregory, 1974, Formation velocity and density; the diagnostic basics for stratigraphic traps: Geophysics, **39**, 770–780, doi: 10.1190/1.1440465.

Hardage, B., D. Carr, D. Lancaster, J. Simmons, Jr, R. Elphick, V. Pendleton, and R. Johns, 1996, 3-D seismic evidence of the effects of carbonate karst collapse on overlying clastic stratigraphy and reservoir compartmentalization: Geophysics, **61**, 1336–1350, doi: 10.1190/1.1444057.

Henry, J. D., 1982, Stratigraphy of the Barnett Shale (Mississippian) and associated reefs in the northern Fort Worth basin: Dallas Geological Society, 157–177.

Keller, G. R., 2009, Some thoughts on the structure and evolution of the Ouachita Mountains–Arkoma basin region: Oklahoma Geology Notes, **69**, 4–12.

Keller, G. R., and S. E. Cebull, 1973, Plate tectonics and the Ouachita system in Texas, Oklahoma and Arkansas: GSA Bulletin, **84**, 1659–1665, doi: 10.1130/0016-7606(1973)84<1659:PTATOS>2.0.CO;2.

Keller, G. R., and R. D. Hatcher, 1999, Some comparisons of the structure and evolution of the southern Appalachian–Ouachita orogen and portions of the Trans-European Suture Zone region: Tectonophysics, **314**, 43–68, doi: 10.1016/S0040-1951(99)00236-X.

Keller, G. R., J. Kruger, K. Smith, and W. Voight, 1989, The Ouachita system: A geophysical overview, *in* R.D. Hatcher, Jr., W. A. Thomas, and G.W. Viele, eds., The Appalachian-Ouachita orogen in the United States, Geology of North America: F-2, Geological Society of America, 689–694.

Kruger, J., and G. R. Keller, 1986, Interpretation of crustal structure from regional gravity anomalies, Ouachita Mountains area and adjacent Gulf Coastal Plain: AAPG Bulletin, **70**, 667–689.

Lahti, I., and T. Karinen, 2010, Tilt derivative multiscale edges of magnetic data: The Leading Edge, **29**, 24–29, doi: 10.1190/1.3284049.

Levine, J., and S. Mosher, 2010, Contrasting Grenville-aged tectonic histories across the Llano uplift, Texas: New evidence for deep-seated high-temperature deformation in the western uplift: Lithosphere, **2**, 399–410, doi: 10.1130/L104.1.

Loucks, R. G., 2003, Review of the Lower Ordovician Ellenburger Group of the Permian basin, West Texas: Bureau of Economic Geology.

Loucks, R. G., and S. C. Ruppel, 2007, Mississippian Barnett Shale: Lithofacies and depositional setting of a deep-water shale-gas succession in the Fort Worth basin, Texas: AAPG Bulletin, **91**, 579–601, doi: 10.1306/11020606059.

Marfurt, K. J., and J. Rich, 2010, Beyond curvature — Volumetric estimates of reflector rotation and convergence, 80th Annual International Meeting, SEG, Expanded Abstracts, 1467–1472.

Meckel, L. D., Jr, D. G. Smith, and L. A. Wells, 1992, Ouachita foredeep basins: Regional paleogeography and habitat of hydrocarbons: *in* R. W. MacQueen, and D. A. Leckie, eds., Foreland basins and fold belts: American Association of Petroleum Geologists, AAPG Memoir, 55, 427–444.

Mickus, K., and G. R. Keller, 1992, Lithospheric structure of the south-central United States: Geology, **20**, 335–338, doi: 10.1130/0091-7613(1992)020<0335:LSOTSC>2.3.CO;2.

Miller, H. G., and V. Singh, 1994, Potential field tilt — A new concept for location of potential field sources: Journal of Applied Geophysics, **32**, 213–217, doi: 10.1016/0926-9851(94)90022-1.

Montgomery, S. L., D. M. Jarvie, K. A. Bowker, and R. M. Pollastro, 2005, Mississippian Barnett Shale, Fort Worth basin, north-central Texas: Gas-shale play with multi-trillion cubic foot potential: AAPG Bulletin, **89**, 155–175, doi: 10.1306/09170404042.

Mosher, S., J. Levine, and W. Carlson, 2008, Mesoproterozoic plate tectonics: A collisional model for the Grenville-aged orogenic belt in the Llano uplift, central Texas: Geology, **36**, 55–58, doi: 10.1130/G24049A.1.

Nicholas, R., and D. Waddell, 1989, The Ouachita system in the subsurface of Texas, Arkansas, and Louisiana, *in* R.D. Hatcher, Jr., W. A. Thomas, and G.W. Viele, eds., The Appalachian-Ouachita orogen in the United States, Geology of North America: F-2, Geological Society of America, 661–672.

Nicholas, R. L., and R. A. Rozendal, 1975, Subsurface positive elements within Ouachita foldbelt in Texas and their relation to Paleozoic cratonic margin: AAPG Bulletin, **59**, 193–216.

Oliver, H. W., 1977, Gravity and magnetic investigations of the Sierra Nevada batholith, California: GSA Bulletin, **88**, 445–461, doi: 10.1130/0016-7606(1977)88<445:GAMIOT>2.0.CO;2.

PACES, 1995, Pan American Center for Earth and Environmental Studies, University of Texas, http://research.utep.edu/Default.aspx?alias=research.utep.edu/paces, accessed 10 June 2010.

Pollastro, R. M., R. J. Hill, D. M. Jarvie, and M. E. Henry, 2003, Assessing undiscovered resources of the Barnett-Paleozoic total petroleum system, Bend arch–Fort Worth Basin province, Texas: Transaction of the AAPG Southwest Section Convention, Fort Worth, Texas, AAPG/Datapages, 18, CD-ROM. http://www.searchanddiscovery.com/documents/pollastro/index.htm, accessed June 2004.

Pollastro, R. M., D. M. Jarvie, R. J. Hill, and C. W. Adams, 2007, Geologic framework of the Mississippian Barnett shale, Barnett-paleozoic total petroleum system, Bend arch–Fort Worth basin, Texas: AAPG Bulletin, **91**, 405–436, doi: 10.1306/10300606008.

Preston, R. D., D. J. Pavilcek, R. L. Bluntzer, and J. Derton, 1996, The Paleozoic and related aquifers of central Texas, Texas Water Development Board, Austin, report 346 77.

Railroad Commission of Texas, 2010, http://www.rrc.state.tx.us/data/online/gis/index.php, accessed 8 August 2010.

Reid, A. B., J. Allsop, H. Granser, A. Millet, and I. Somerton, 1990, Magnetic interpretation in three dimensions using Euler deconvolution: Geophysics, **55**, 80–91, doi: 10.1190/1.1442774.

Schuelke, J. S., 2011, Overview of seismic attribute analysis in shale play: Attributes: New views on seismic imaging — Their use in exploration and production, Presented at 31st Annual GCSSEPM Foundation Bob F. Perkins Research Conference.

Smith, R., 2004, Paleozoic aquifers of the Llano Uplift: Aquifers of the Edwards Plateau: Texas Water Development Board Report, 360, 181–200.

Sullivan, E. C., K. J. Marfurt, A. Lacazette, and M. Ammerman, 2006, Application of new seismic attributes to collapse chimneys in the Fort Worth basin: Geophysics, **71**, no. 4, B111–B119, doi: 10.1190/1.2216189.

Tai, D. T. W., 1979, Subsurface study of Atoka (Lower Pennsylvanian) clastic rocks in parts of Jack, Palo Pinto, Parker, and Wise counties, north-central Texas: AAPG Bulletin, **63**, 50–66.

Thomas, J. D., and W. Texas, 2003, Integrating synsedimentary tectonics with sequence stratigraphy to understand the development of the Fort Worth basin: Presented at AAPG Southwest Section Meeting, http://www.searchanddiscovery.com/abstracts/pdf/2003/2002sw/image/ndx_thomas.pdf.

Thompson, D., 1982, EULDPH: A new technique for making computer-assisted depth estimates from magnetic data: Geophysics, **47**, 31–37, doi: 10.1190/1.1441278.

Verduzco, B., J. D. Fairhead, C. M. Green, and C. MacKenzie, 2004, New insights into magnetic derivatives for structural mapping: The Leading Edge, **23**, 116–119, doi: 10.1190/1.1651454.

Viele, G. W., 1989, The Ouachita orogenic belt, *in* R.D. Hatcher, Jr., W. A. Thomas, and G.W. Viele, eds., The Appalachian-Ouachita orogen in the United States, Geology of North America: F-2, Geological Society of America, 555–561.

Viele, G. W., and W. A. Thomas, 1989, Tectonic synthesis of the Ouachita orogenic belt, *in* R.D. Hatcher, Jr., W. A. Thomas, and G.W. Viele, eds., The Appalachian-Ouachita orogen in the United States, Geology of North America: F-2, Geological Society of America, 692–726.

Walper, J. L., 1982, Plate tectonic evolution of the Fort Worth basin, *in* C. A. Martin, ed., Petroleum geology of the Fort Worth Basin and Bend Arch Area: Dallas Geological Society, 237–251.

Murari Khatiwada received a master's degree in geology from Tribhuvan University, Nepal, and an M.S. in geophysics from Boise State University. He is a Ph.D. candidate in geophysics and a graduate research assistant at the University of Oklahoma. His research is focused on integrating a variety of geophysical, geospatial, and well-log data for geologic and tectonic study of basins to the crustal scale structures in various tectonic settings. He has served as one of the SEG student chapter officers at Boise State University and the University of Oklahoma and has received several SEG scholarships and other departmental scholarships. He won first place in the fifth regional SEG challenge bowl. He also won one of the best student research abstract prizes at the 2012 AAPG annual meeting in Long Beach, California.

G. Randy Keller is a professor in the School of Geology and Geophysics at the University of Oklahoma and the holder of the Edward Lamb McCollough Chair in Geophysics. He also serves as the director of the Oklahoma Geological Survey and is a State Geologist. His research interests stress the geologic applications of geophysics and span a variety of techniques at a variety of scales. Keller, his students, and colleagues have conducted many studies of the structure and evolution of the crust using gravity, magnetic, remote sensing, and seismic measurements integrated with geologic data, often as part of large international cooperative efforts. They have also regularly used geophysical methods to study topics such as groundwater resources, earthquake hazards, the geometry of specific geologic structures, and site characterization. His international research has focused on East Africa, North Africa, Central Europe, and China. He has been active in SEG and AAPG and was awarded the Grover E. Murray Memorial Distinguished Educator Award by AAPG.

Kurt J. Marfurt joined the University of Oklahoma in 2007, where he serves as the Frank and Henrietta Schultz Professor of Geophysics within the ConocoPhillips School of Geology and Geophysics. His primary research interest is in the development and calibration of new seismic attributes to aid in seismic processing, seismic interpretation, and reservoir characterization. His recent work has focused on correlating seismic attributes such as volumetric curvature, impedance inversion, and azimuthal anisotropy with image logs and microseismic measurements with a particular focus on resource plays. In addition to his teaching and research duties at OU, Marfurt leads short courses on attributes for SEG and AAPG.